Rotational radial shear in the low solar photosphere

M. Faurobert, Thierry Corbard, B. Gelly, R. Douet, D. Laforgue

A&A 676, L4 (2023)
https://doi.org/10.1051/0004-6361/202346610

Astronomy & Astrophysics

LETTER TO THE EDITOR

Rotational radial shear in the low solar photosphere

M. Faurobert[1], T. Corbard[1], B. Gelly[2], R. Douet[2], and D. Laforgue[2]

[1] Université Côte d'Azur, Observatoire de la Côte d'Azur, CNRS UMR 7293, J.L. Lagrange Laboratory, Campus Valrose, 06108 Nice, France
e-mail: marianne.faurobert@oca.eu; thierry.corbard@oca.eu
[2] CNRS-IRL2009, c/o IAC Via Lactea s/n, 38205 La Laguna, Tenerife, Spain
e-mail: bgelly@themis.iac.es

Received 6 April 2023 / Accepted 14 July 2023

ABSTRACT

Context. Radial differential rotation is an important physical ingredient in stellar dynamo theory. In the case of the Sun, heliosismology techniques have revealed the existence of a near-surface shear layer covering 15–20% of the upper convection zone. It was recently shown that the rotation velocity gradient is not uniform in this layer and that it displays a steep increase in a shallow layer near the surface.
Aims. We report the detection of a rotation velocity depth-gradient in the low photosphere that is not accessible to heliosismology techniques.
Methods. We applied differential interferometric methods to spectroscopic data obtained with the solar telescope THEMIS, which is equipped with an efficient adaptative optics system. The detection was based on the measurement of a systematic east-west shift between images of the solar granulation at different depths in the FeI 630.15 nm at the center of the solar disk. The same technique was applied to obtain the depth-difference between the images from their perspective shift when they are observed away from the disk center. Both THEMIS and HINODE/SOT data were used for the height-difference measurement, giving similar results.
Results. At the center of the solar disk, we measured a systematic retrograde shift of the photospheric granular structures on the east-west axis and with no shift in the north-south direction. The retrograde shift increases linearly with height. We interpret these findings as a signature of a steep decrease in the angular velocity in the low photosphere.
Conclusions. The rotational radial shear in the low solar photosphere is likely related to the dynamics of the subsurface shear layer. Its measurement yields a valuable constraint on the numerical simulations of the solar upper convection zone.

Key words. techniques: high angular resolution – techniques: spectroscopic – Sun: photosphere

1. Introduction

Rotational shear plays a major role in driving the stellar dynamo. In the Sun, helioseismic observations have revealed two regions that show a strong height-gradient of the rotation rate, namely, the tachocline at the base of the convective zone and the near surface shear layer (NSSL).

By using only observations of surface gravity modes (f-modes), observed by the Michelson Doppler Imager (MDI) onboard the Heliospheric Observatory (SoHO), Corbard & Thompson (2002) were able to obtained a clean measurement of the mean radial gradient of the angular velocity in the subsurface layer, from about 4 Mm below the surface down to 9 Mm. More recent global and local helioseismology results (e.g., Zaatri & Corbard 2009; Reiter & Rhodes 2020; Komm 2022) covering longer periods and a full solar cycle have confirmed that the gradient of rotation is not uniform in the NSSL and that the rotation rate exhibits a steep decrease close to the surface (see Komm 2022, Fig. 5).

On the theoretical side, in a recent paper devoted to radiative hydrodynamic numerical simulations of the near-surface of the sun in the presence of rotation, Kitiashvili et al. (2023) derived a strong negative gradient in the angular velocity of $\partial \ln \Omega / \partial \ln r \simeq -4$ in a subsurface layer at depths smaller than 4 Mm.

In the present work, we are interested in the rotation profile of the photospheric layer. The photospheric rotational velocity derived from the measurement of the rotation of sunspot or via the Doppler velocity of spectral lines show systematic differences, which indicate that the photospheric plasma rotates at a slower rate than the sunspots. This effect has been explained as a result of a difference in rotational velocities between the surface and subsurface layers (see Foukal 1972). The active regions anchored below the photosphere would thereby rotate faster than the photospheric plasma. Depth variations in the rotational velocity have been investigated in Livingston & Milkey (1972) by spectroscopic methods, without yielding any evidence of a depth gradient. However, using a new analysis of 5 mn solar p-mode limb oscillations from 3.5 yr of the Helioseismic and Magnetic Imager (HMI) data, Cunnyngham et al. (2017) measured a steep radial decrease of the latitudinal average of the solar rotation rate in the upper photosphere. These authors argued that angular momentum loss could be driven by the torque due to the escape of photons from the photosphere. In this work, we report the detection of a steep rotational shear at the equator in the low photosphere.

The detection relies on the measurement of systematic shifts between simultaneous images of the granulation taken at different altitudes. The images are related to the temperature fluctuations of the granulation pattern. They form coherent structures that we have observed simultaneously at different altitudes. In the field of view (along the spectrograph slit and at many slit positions), we have observed a large number of structures.

To extract statistical information on possible systematic shifts, we opted against tracking the evolution of the individual structures and instead we performed ensemble averages of the cross-spectra among simultaneous images at different levels. In this context, systematic refers to the fact that the ensemble average is different from zero. Such systematic shifts may arise from two different effects, namely, a perspective effect in the radial direction when the images are taken away from the center of the solar disk or horizontal shifts that are induced by a height-gradient of large scale horizontal velocities projected on the plane of the sky. Other kinds of turbulent motions would not lead to any measurable systematic shift. The horizontal shift of a structure is proportional to the duration of the dragging of the upper layer by the velocity gradient namely, to the correlation time of the granulation pattern. We discuss this issue in greater detail in the following.

We use x and y to denote the coordinates in the heliocentric west-east and south-north axis. The x-axis is oriented in the direction of the solar rotation, while the y-axis points toward the north. We started by considering the regions along the polar axis ($x = 0$) and the shift has two components that are given as:

$$\Delta x = \Delta v_\varphi \cos\theta\,\tau,$$
$$\Delta y = z\sin\theta + \Delta v_\theta \cos\theta\,\tau. \quad (1)$$

For regions located along the east-west axis ($y = 0$), we have:

$$\Delta x = \Delta v_\varphi \cos\theta\,\tau + z\sin(\theta),$$
$$\Delta y = \Delta v_\theta \cos\theta\,\tau, \quad (2)$$

where θ denotes the heliocentric angle, z is the difference of the image formation heights, Δv_φ and Δv_θ are the difference of the azimuthal and meridional velocities at the two heights, respectively, and τ is the characteristic coherence time of the granulation pattern.

In this Letter, we report the detection at the center of the solar disk of systematic negative shifts along the equator, with no measurable shifts along the south-north axis. The equatorward shifts vary linearly with the altitude in the low photosphere. We interpret these findings as a signature of a decrease in the rotational velocity with height. In the next section (Sect. 2), we present our observations and methods. Section 3 is devoted to the measurement of the perspective shift from THEMIS and HINODE spectroscopic data. Section 4 describes the longitudinal shift observed at the center of the solar disk. In Sect. 5, we draw our conclusions and offer perspectives.

2. Observations and methods

We used spectroscopic observations obtained at the solar telescope THEMIS dating from July 18 to July 22, 2022, in the FeI 630.15 nm line. We performed a data reduction following Wöhl et al. (2002). We also used HINODE Solar Optical Telescope (SOT) spectropolarimetric (SP) data from the irradiance program, HOP79, performed on July 21, 2022. With THEMIS, we scanned $40'' \times 108''$ quiet solar regions at different positions along the west-east central axis with the spectrograph slit oriented along the west-east direction, and along the south-north polar axis with the slit oriented along the south-north direction. The slit width was $0.5''$ and the scan step one arcsecond. The HOP79 irradiance program performs monthly systematic scans of $30'' \times 130''$ regions at 20 positions along the polar axis, covering the solar diameter from the north to the south limb with the spectrograph slit oriented along the south-north direction. The pixel size along the slit is $0.235''$ at THEMIS and $0.32''$ on SOT-SP, the spectral pixel is 1.35 pm at Themis and 2.1 pm on SOT-SP. A clear advantage of HINODE is the absence of seeing-induced image degradation. With respect to THEMIS, we were able to benefit from some good weather conditions and of the Adaptative Optic system (AO; Thiébaut et al. 2022; Gelly et al. 2016), we further selected the best spectrograms with a quality criteria based on the root mean square (rms) contrast of the granulation in the continuum along the slit.

To measure a very small displacement between images in the continuum and in the line-wings, we used the phase of their cross-spectrum. This method requires us to consider the power spectra of intensity fluctuations in images taken rigorously at the same time in the continuum and in the line. Actually, 2D images are not needed as far as the spectrograph slit is oriented in the direction of the displacement. In practice, we used 1D power spectra of the intensity variations along the spectrograph slit and we summed over all the slit positions. Using $I_i(x)$ and $I_c(x)$ to denote the 1D cuts of the line-wing and continuum images, respectively, and assuming that the line-wing image is similar to the continuum one, but slightly displaced at a distance δ, we can express the following:

$$I_i(x) \sim I_c(x-\delta), \quad (3)$$

and subsequently,

$$\widehat{I_i}(u) \sim \widehat{I_c}(u)\exp(2i\pi u\delta). \quad (4)$$

Shifts can then be derived from the phase of the cross-spectrum. We used a series of spectrograms to estimate the cross-spectrum $\widehat{Q_{ci}}$ between $I_c(x)$ and $I_i(x)$:

$$\widehat{Q_{ci}}(u) = \langle \widehat{I_c}(u)\widehat{I_i^*}(u)\rangle \sim \langle |\,\widehat{I_c}(u)\,|^2\rangle e^{-2i\pi\delta u}, \quad (5)$$

where $\widehat{I_i^*}(u)$ represents the conjugate Fourier transform of $I_i(x)$ and the brackets refer to the ensemble average. A linear fit of the phase variation with respect to the spatial frequency variable, u, allows us to measure δ. We note that a positive shift corresponds to a negative slope of the phase. We stress here that this method is not limited by the spatial resolution of the instrument. The main limitation is the signal-to-noise ratio (S/N) of the image spectrum and the domain of validity of Eq. (3), which is based on the assumption of similarity between the line-wing and continuum images.

To apply this method, we want to construct images formed on surfaces at a roughly constant continuum optical depth. Our reconstruction method relies on the relation between the line and continuum absorption coefficients in the Lorentzian damping wings of a line. This is presented in detail and applied to Hinode/SOT data in Faurobert et al. (2012). Here, we apply it to both the SOT-SP and THEMIS data.

As ground-based THEMIS spectra are affected by the presence of telluric lines in the far wings of the FeI 603.15 nm line, we implemented a procedure to restore the shape of the line intensity profile in the line wings. Because of the asymmetry introduced by the telluric line on the top of the red wing side (see Fig. 1), we decided to fit the two parts of the profile separately. First, the location of the line core, λ_0, and the intensity value, I_0, at the line core are obtained accurately from the whole profile using cubic convolution interpolation. Then both sides of the profile are symmetrized and fitted by two independent symmetric Voigt profiles. Finally, the whole profile is thus represented by a total of nine parameters: Gaussian (Doppler) and Lorentzian

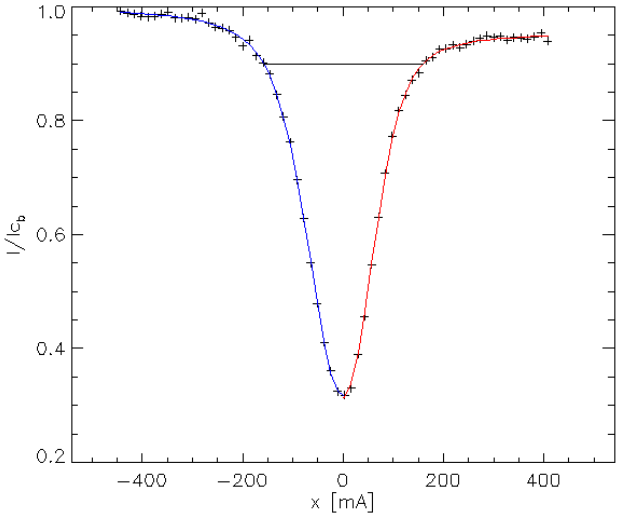

Fig. 1. Example of line fit by two half Voigt profiles. Crosses represent the data points. The horizontal line shows the full line width at intensity level 0.9 I_c, where I_c is the continuum level estimated from the blue wing.

widths, integrated line strengths and wing intensity levels on the red and blue sides, plus the line core intensity value. The intensity level obtained on the blue wing is considered as a reliable estimate of the continuum level, I_c, because there is no contamination by telluric or other solar lines on that side. The red wing intensity level is always lower than I_c and we rejected data for which it is lower than $0.9\,I_c$.

As in the study by Faurobert et al. (2012), we obtained images at 25 line-cords of evenly distributed widths between the line center (line cord 1) and the line wing at $0.9I_c$ (line cord 25) that is taken as the reference image in the following.

3. Perspective-shift measurement from Hinode and Themis data

First, we applied the method described above to images taken along the y axis with the spectrograph-slit oriented in the y direction. Figure 2 shows the phase of the cross-spectrum of the reference image and the image at line cord 16 with both SOT/SP (red symbols) and THEMIS (blue symbols) at $\cos\theta = 0.74$. We note that the phase shows a linear behavior at spatial frequencies typically smaller than $0.6\,\mathrm{arsec}^{-1}$, corresponding to structures at scales larger than $1.7''$. A linear fit of the phase in this spatial-frequency interval is shown in the figure. At larger frequencies, (i.e., on smaller scales), the cross-spectrum phase is noisy for two reasons: (1) the assumption of similarity between the images is no longer valid because small structures tend to evolve more quickly and to lose coherency between the two altitudes and (2) the S/N of the Fourier power spectrum of the images decreases at high spatial frequencies. As expected from the perspective shift, the sign of the phase-slope is negative for regions located in the northern hemisphere and positive for regions located in the southern hemisphere. The results obtained with HINODE and THEMIS data are in good agreement. Table 1 shows the heights z derived from the measurement of the phase-slope up to line-cord 14 from different observation sequences.The standard deviation on the measurement is derived from the standard deviation on the estimate of the slope of the linear fit. At line-cords deeper than 14, the assumption of similarity with the reference image is no longer valid and the cross-spectrum phase becomes too noisy for a reliable measurement. To take into account the quality of the different measurements, we considered the average of z weighted with the inverse of the variance of the individual measurements.

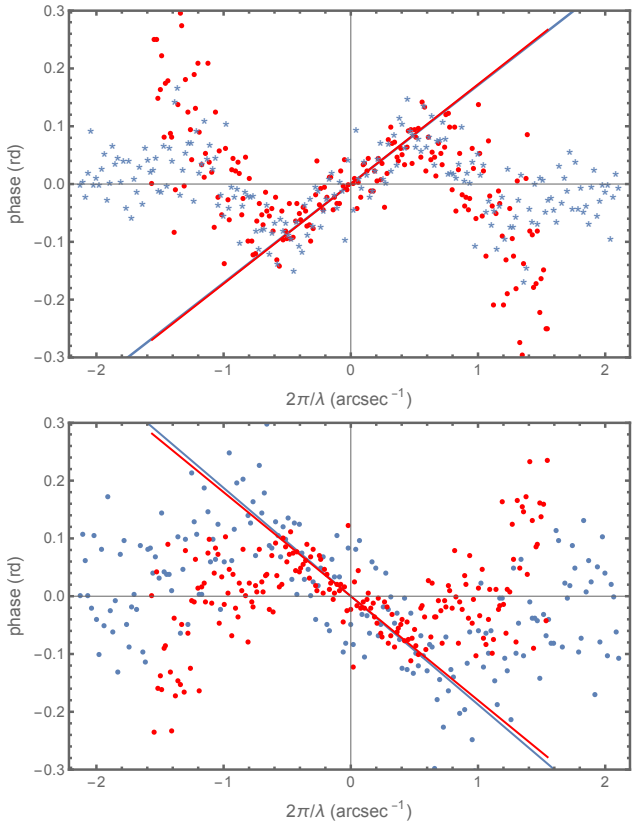

Fig. 2. Phase of the cross-spectrum of the images at the reference level and at line cord 16 as function of the spatial frequency. The spectrograph slit is oriented along the north-south axis. Red symbols: results obtained with the Hinode data (in blue: Themis data). Upper panel: results for regions at $\cos\theta = 0.74$ in the southern hemisphere on the solar polar axis. Lower panel: results at $\cos\theta = 0.74$ in the northern hemisphere.

Figure 3 shows the cross-spectrum phase obtained at the center of the solar disk, where the perspective shift vanishes. The spectrograph slit is oriented along the y direction. The phase remains close to zero and shows a noisy behavior, while the measured shift is close to 0. This shows that the measurements are not significantly affected by a possible gradient of the meridional velocity or by any depth-gradient of large scale supergranular flows that are not detectable here.

4. Measurement of the height-gradient of the azimuthal velocity

The same method was then applied to images obtained at the center of the solar disk where the perspective shift vanishes. The slit in this case is oriented along the west-east axis. Figure 4 shows the cross-spectrum phase from three sequences of observations performed on July 19, 20, and 22, 2022, for line-wings images at line cords 16 and 18. We note a linear behavior of the phase at spatial frequencies smaller than $0.6\,\mathrm{arsec}^{-1}$ with a positive slope that remains approximately constant for the three sequences; this is the evidence of a systematic displacement of the structures seen above the continuum level. The shifts derived from the slope of the linear part are given in Table 2 for different line cords.

Table 1. Northfhward shifts (in km) of the granulation images observed at $\cos(\theta) = 0.74$ in the northern hemisphere with the spectrograph slit oriented along the south-north axis.

Line cord	2022/07/20	2022/07/22	Hinode 2022/07/21	Weighted average z (km)
20	8.2 ± 0.7	9.5 ± 0.7	7.7 ± 1.4	8.7 ± 0.5
18	13.8 ± 0.7	13.8 ± 0.7	13.4 ± 1.4	13.8 ± 0.4
16	22.7 ± 2.4	21.5 ± 1.0	21.1 ± 1.9	21.6 ± 0.9
15	28.2 ± 1.4	26.1 ± 9.2	28.8 ± 1.8	28.4 ± 1.1
14	30.7 ± 2.4	34.6 ± 9.4	33.3 ± 2.1	32.4 ± 1.4

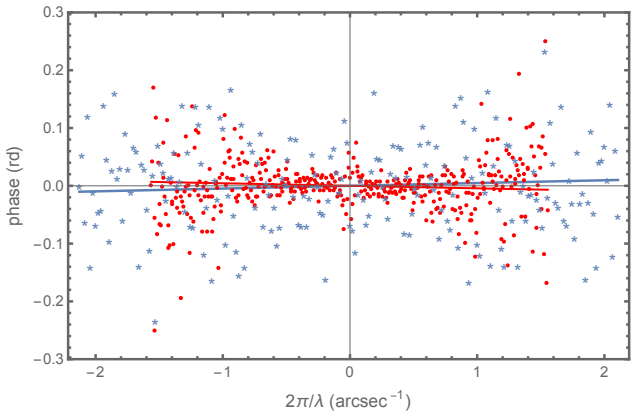

Fig. 3. Same as Fig. 2, but for a region at the center of the solar disk.

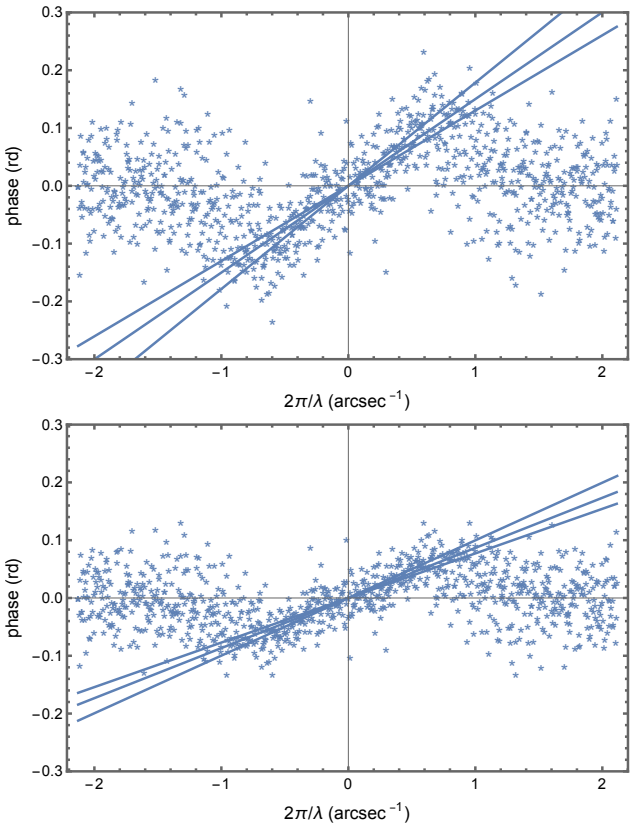

Fig. 4. Phase of the cross-spectrum as function of the spatial frequency for three observing sequences. The observed regions are at the center of the solar disk and the spectrograph slit is oriented along the west-east axis. The straight lines show linear fits of the phase at spatial frequency smaller than 0.6 arcsec^{-1}. Upper panel: cross-spectrum phase of the reference image and image at line cord 16. Lower panel: same for line cord 18.

Figure 5 shows that the longitudinal shift varies linearly with the altitude. Let us assume that the granular structures are dragged by a linearly decreasing angular velocity $\Omega(R + z) = \Omega(R)(1 - \alpha z)$, where R denotes the solar radius at the depth of our reference image. The rotational velocity at the altitude z is then given by $v_{\rm rot}(R + z) = (R + z)\Omega(R + z)$, at a first order in z/R we get $v_{\rm rot}(R + z) = v_{\rm rot}(R)(1 + z/R)(1 - \alpha z)$. Measurable shifts are obtained only if $\alpha \gg 1/R$. The shift Δx at the altitude z is then given by:

$$\Delta x = -v_{\rm rot}(R)\,\tau\,\alpha\,z. \tag{6}$$

The slope of the linear fit in Fig. 5 is -0.79. The rotational velocity at the solar surface is around 2 km s^{-1}, which gives $\alpha = 0.79/(2\tau)$ (km^{-1}). The estimate of α depends on the coherence time of the structures that give rise to the signal. As the intensity variations along the spectrograph slit are dominated by the granulation, we may identify τ with the correlation time of the granulation pattern. A value of 440 s was estimated for this quantity in Title et al. (1988). This is close to the average lifetime of granular structures, which is on the order of 600 s (Roudier et al. 2012), this gives $\alpha \simeq 9 \times 10^{-4}$ km^{-1}. However, many solar observations have shown the existence of "trees of fragmenting granules" (TFG; Roudier et al. 2003, 2009; Malherbe et al. 2015) that cover a significant fraction of the solar surface and can live much longer than individual granules. The lifetime histogram of the TFG may be fitted by an exponentially decreasing law with a timescale of about one hour. We remark that the signal we observe is stationary on several days, indicating that in our field of view of 40″ by 108″ we have statistically stable TFG distributions. However, the identification of the TFGs would require us to obtain images of the field of view at a constant time-step for more than one hour. This could be done from space with SDO/HMI. One advantage of the method applied here is that we do not need to work with 2D images taken at constant time-step, which allows us to perform a selection of the best spectrograms based on a contrast criterion. However, we are not able to follow the evolution of the pattern that gives rise to the signal.

5. Discussion and conclusions

By using a differential interferometric technique, we were able to measure small systematic negative longitudinal shifts of granular structures taken at different heights in the low solar photosphere at the center of the solar disk. No shifts were detected along the south-north direction. The measurement of the formation heights of the images was obtained from the perspective shifts observed away from the center of the solar disk. We find that the longitudinal shift varies linearly with height. The

Table 2. Longitudinal shifts (in km) of the images observed at the center of the solar disk at different line cords for three sequences of observations with the spectrograph slit oriented along the west-east axis.

Line cord	2022/07/19	2022/07/20	2022/07/22	Weighted average Δx (km)
20	-5.0 ± 0.6	-5.0 ± 8.8	-5.5 ± 7.5	-5.0 ± 0.6
18	-9.0 ± 0.7	-11.7 ± 0.7	-10.2 ± 0.7	-10.3 ± 0.4
16	-14.6 ± 1.3	-20.0 ± 1.2	-16.2 ± 1.1	-18.7 ± 0.7
15	-20 ± 11.8	-25.5 ± 9.7	-22.3 ± 1.3	-22.3 ± 1.3
14	-24.9 ± 2.4	-33.4 ± 9.9	-28.2 ± 1.9	-27.1 ± 1.6

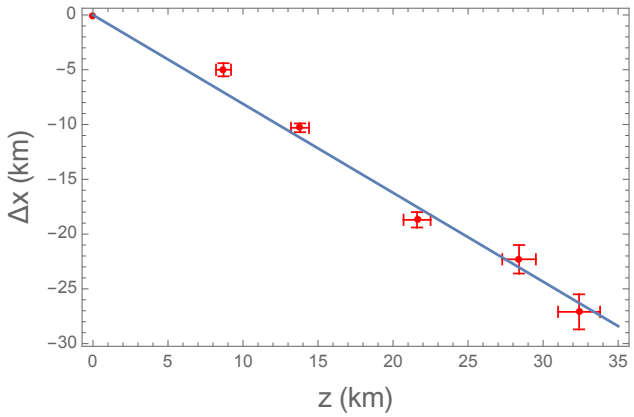

Fig. 5. Relation between the longitudinal shift of the images and the image formation height. The straight line shows a linear fit.

measurements were performed in a thin layer of 30 km in the low photosphere. We interpret these observations as the signature of a negative height gradient of the angular velocity of the following form: $\Omega(R + z) = \Omega(R)(1 - \alpha z)$.

Estimating the value of α requires the knowledge of the coherence time of the pattern that gives rise to the observed signal. Identifying this time to the correlation time of the granulation we obtain $\alpha \simeq 9 \times 10^{-4}\,\mathrm{km}^{-1}$. However, longer lived features, such as TFGs, could be at the origin of the signal we detected, which would decrease our estimate of the rotational depth-gradient. We leave this point to further studies.

We may compare our results to the angular velocity measurements at the solar limb reported in Cunnyngham et al. (2017), Table 1. A linear fit of their measurements gives $\alpha \simeq 2 \times 10^{-4}\,\mathrm{km}^{-1}$. This is more than four times smaller than our estimated value, but we note that we measured the rotational shear at the equator – whereas they measured a latitudinal average over some effective depths. We agree with their own comments on their results, asserting that "depth and latitude smearing will spatially average the local rotation gradient" and we agree that studies at a higher resolution like ours may detect a larger rotation gradient.

As our observations were performed at the equator of the Sun, in future works, we intend to investigate possible latitudinal variations of the angular velocity gradient and to extend the measurement to higher layers of the photosphere.

Acknowledgements. This work was supported by the Programme National PNST of CNRS/INSU co-funded by CNES and CEA. Hinode is a Japanese mission developed and launched by ISAS/JAXA, collaborating with NAOJ as a domestic partner, NASA and STFC (UK) as international partners. Scientific operation of the Hinode mission is conducted by the Hinode science team organized at ISAS/JAXA. This team mainly consists of scientists from institutes in the partner countries. Support for the post-launch operation is provided by JAXA and NAOJ (Japan), STFC (UK), NASA, ESA, and NSC (Norway).

References

Corbard, T., & Thompson, M. J. 2002, Sol. Phys., 205, 211
Cunnyngham, I., Emilio, M., Kuhn, J., Scholl, I., & Bush, R. 2017, Phys. Rev. Lett., 118, 051102
Faurobert, M., Ricort, G., & Aime, C. 2012, A&A, 548, A80
Foukal, P. 1972, ApJ, 173, 439
Gelly, B., Langlois, M., Moretto, G., et al. 2016, in Ground-based and Airborne Telescopes VI, eds. H. J. Hall, R. Gilmozzi, & H. K. Marshall, SPIE Conf. Ser., 9906, 99065A
Kitiashvili, I. N., Kosovichev, A. G., Wray, A. A., Sadykov, V. M., & Guerrero, G. 2023, MNRAS, 518, 504
Komm, R. 2022, Front. Astron. Space Sci., 9, 1017414
Livingston, W., & Milkey, R. 1972, Sol. Phys., 25, 267
Malherbe, J. M., Roudier, T., Frank, Z., & Rieutord, M. 2015, Sol. Phys., 290, 321
Reiter, J., Rhodes, E. J., J., Kosovichev, A. G., , et al. 2020, ApJ, 894, 80
Roudier, T., Lignières, F., Rieutord, M., Brandt, P. N., & Malherbe, J. M. 2003, A&A, 409, 299
Roudier, T., Rieutord, M., Brito, D., et al. 2009, A&A, 495, 945
Roudier, T., Rieutord, M., Malherbe, J. M., et al. 2012, A&A, 540, A88
Thiébaut, É., Tallon, M., Tallon-Bosc, I., et al. 2022, in Adaptive Optics Systems VIII, eds. L. Schreiber, D. Schmidt, & E. Vernet, International Society for Optics and Photonics (SPIE), 12185, 1218507
Title, A., Tarbell, T., Topka, K., et al. 1988, Astrophys. Lett. Commun., 27, 141
Wöhl, H., Kučera, A., Rybák, J., & Hanslmeier, A. 2002, A&A, 394, 1077
Zaatri, A., & Corbard, T. 2009, in Solar-Stellar Dynamos as Revealed by Helio- and Asteroseismology: GONG 2008/SOHO 21, eds. M. Dikpati, T. Arentoft, I. González Hernández, C. Lindsey, & F. Hill, ASP Conf. Ser., 416, 99